

Moiré superlattice and two-dimensional free-electron-like states of indium triple-layer structure on Si(111)

Shinichiro Hatta^{✉,*}, Kenta Kuroishi^{✉,†}, Keisuke Yukawa, Tomoka Murata,
Hiroshi Okuyama^{✉,‡}, and Tetsuya Aruga[✉]

Department of Chemistry, Graduate School of Science, Kyoto University, Kyoto 606-8502, Japan

 (Received 2 June 2023; revised 10 July 2023; accepted 13 July 2023; published 31 July 2023)

We studied the growth of an indium triple-atomic-layer film and the two-dimensional free-electron-like electronic states on Si(111) by low-energy electron diffraction (LEED), scanning tunneling microscopy (STM), and angle-resolved photoelectron spectroscopy (ARPES). By depositing In on the In/Si(111)- $\sqrt{7} \times \sqrt{3}$ -rect surface below 100 K, followed by brief postannealing up to 140 K, we successfully obtained well-crystalline films exhibiting sharp superstructure LEED spots. We revealed an (11×11) superlattice of the triple-layer structure, while both LEED and STM showed a (5.5×5.5) pseudoperiodicity. This pseudoperiodicity was attributed to the moiré interference between the Si(111)- (11×11) lattice ($a = 3.84 \text{ \AA}$) and the In (13×13) hexagonal lattice, which has a lattice constant of 3.25 \AA , with the ratio very close to $13/11$. ARPES measurements unveiled two free-electron-like states with Fermi wave vectors of 1.32 and 1.46 \AA^{-1} . We also observed replica Fermi surfaces, which are associated with the reciprocal lattice vectors of both the (1×1) Si(111) and the In hexagonal layers. This further confirms the hexagonal atomic arrangement of the In triple-layer structure.

DOI: [10.1103/PhysRevB.108.045427](https://doi.org/10.1103/PhysRevB.108.045427)

I. INTRODUCTION

The quantum properties of ultrathin metal films have generated significant interest due to the sensitivity of confined electronic states to subtle differences in film thickness. This sensitivity has enabled control over superconducting states [1], surface reactivity [2], and optical properties associated with collective electronic excitations [3]. The achievement of highly crystalline metal films on semiconductor substrates is crucial for quantum confinement of metallic electronic states. However, this has been demonstrated only in limited combinations of semiconductor substrates and metals. Small variations in the bonding of constituent atoms can result in noncrystalline growth of the initial monolayer, posing challenges in obtaining well-defined electron confinement. In this context, the In/Si interface is particularly intriguing. It facilitates the formation of few-layer crystalline In films on Si(111) with atomically flat interfaces simply by depositing In on a reconstructed Si(111) surface while controlling the substrate temperature [4–12]. The term “In films” assumes atomic layers whose net densities are comparable to bulk In and thus, it usually does not include some superstructures on In/Si(111) at monolayer or submonolayer coverages, such as $\sqrt{3} \times \sqrt{3}$ ($\frac{1}{3}$ ML [13]) and 4×1 (1 ML [14]), where ML is defined as the atomic density of the Si(111)- (1×1) surface.

The thinnest known indium film on Si(111) is the so-called “hex” structure where a single-layer structure has an incommensurate lattice very close to a $\sqrt{7} \times \sqrt{3}$ superlattice. The coverage is 1.4 ML [9,11,15]. Note that the metallic radius of

In atoms (3.25 – 3.38 \AA in bulk In) is 85%–88% of the lattice constant $a_{\text{Si}} = 3.84 \text{ \AA}$ of the Si(111)- (1×1) . This size difference results in a higher atomic density of 1.4 ML in the In single layer. The single-layer film confines two-dimensional (2D) free-electron-like states which exhibit metallicity at ambient temperatures. However, upon cooling, it undergoes a metal-insulator transition at around 250 K.

The thinnest In film that maintains metallicity even at the lowest temperatures is a double-layer structure known as the $\sqrt{7} \times \sqrt{3}$ -rect superstructure [5]. This structure consists of two layers with a coverage of 1.2 ML each, forming a quasirectangular lattice [8,10,16]. This film undergoes a superconducting transition at 3 K [6] and exhibits typical properties associated with 2D superconductors [7,12,17]. The atomic arrangement of this film closely resembles that of bulk In, which adopts a body-centered tetragonal (bct) structure. This similarity raises the possibility of further growth of bct(001) films upon additional deposition. However, previous studies [18–20] have reported the preferential growth of three-dimensional (3D) islands at and above room temperature. As a result, the growth of thicker films has been considered challenging.

The epitaxial growth is governed by both energetics and kinetics. To achieve the growth of triple-layer or thicker In films, which may be stable or metastable but not achievable under typical deposition conditions, the surface diffusion of In atoms should be controlled by cooling the $\sqrt{7} \times \sqrt{3}$ -rect substrate [20–22]. By employing this approach, a (6×6) superstructure was found to fully cover the $\sqrt{7} \times \sqrt{3}$ -rect structure at a total coverage of ~ 4 ML [20].

A scanning tunneling microscopy (STM) study indicates an epitaxial growth of hexagonal In layers in lattice matching between $6a_{\text{Si}}$ and $7a_{\text{In}}$ [21]. Other STM studies have also reported similar superstructures, (5.5×5.5) and $(\sim 5.4 \times \sim 5.4)$

*hatta@kuchem.kyoto-u.ac.jp

†Kkenta@surf.kuchem.kyoto-u.ac.jp

‡hokuyama@kuchem.kyoto-u.ac.jp

(Kraft *et al.*, 1997; Suzuki *et al.*, 2022). The detailed lattice relationship among these superstructures has not yet been clarified.

On the other hand, it was reported that the allotropic transition of In films, from fcc to bct, occurs until 10 ML on other substrates [23,24]. The comprehensive characterization of atomic and electronic structures of the intermediate hexagonal layers is crucial to understand the growth process and the properties of ultrathin In films.

In this paper, we present a detailed analysis of the triple-layer structure by STM, low-energy electron diffraction (LEED), and angle-resolved photoelectron spectroscopy (ARPES). Bias-voltage-dependent STM images revealed a hidden superlattice of (11×11) , which was also confirmed by the analysis of the LEED spot pattern. The long periodicity is due to a small mismatch between the Si and In lattices, which are in the relation of $11a_{\text{Si}} = 13a_{\text{In}}$. The registry between the In and the Si atoms yields a moiré modulation with a pseudoperiodicity (5.5×5.5) , which is a half of (11×11) . We found two concentric 2D free-electron-like Fermi surfaces (FSs) for the triple-layer structure. The observed replica FSs indicate comparable contributions from umklapp scatterings by the Si(111) and In hexagonal lattices.

II. EXPERIMENT

Experiments were performed in ultrahigh vacuum (UHV) chambers with base pressures below 1.2×10^{-8} Pa. LEED patterns were acquired with LEED optics (OCI, BDL600IR) and high-sensitivity CMOS cameras. STM observation was performed with a low-temperature STM (USM1200, Unisoku) at 5 and 78 K using a commercial Ag tip. All topographic images shown here were acquired in the constant-current mode. ARPES measurements were performed at 80 K using a hemispherical electron energy analyzer (R3000, VG Scienta) and monochromatized He I (21.2 eV) radiation. The typical energy resolution of the photoelectron spectra was set to 40 meV and the angular resolution 0.1° . The position of the Fermi level (E_{F}) was determined by the Fermi edge of the spectrum from the Ta foil in contact with the sample.

Si(111) substrates were cut from *n*-type Si(111) wafers ($\rho < 0.02 \Omega \text{ cm}$) and were cleaned in each UHV chamber by repeated flash annealing up to 1320–1500 K. An evaporator of In was made with an alumina crucible heated by a tungsten wire loop. The deposition rate was calibrated according to the LEED observation of the In/Si(111)- (4×1) (1.0 ML) and -hex (1.4 ML) phases. The In/Si(111)- $\sqrt{7} \times \sqrt{3}$ -rect structure was prepared by 3-ML deposition and postannealing at 673 K. High crystalline quality of the double-layer film was checked by LEED or STM. Extra In atoms coalesced to form 3D crystals, which density was determined by STM to be very low ($\lesssim 1 \mu\text{m}^{-2}$).

We first investigated the growth of the triple-layer structure by LEED for as-deposited films while keeping the substrate temperature constant. The growth rate was found to depend on substrate temperature; for a deposition rate of 0.3 ML/min, the $\sqrt{7} \times \sqrt{3}$ -rect structure was fully replaced with the triple-layer structure at ≤ 120 K by 1.2 ML (Fig. 1), while above ~ 140 K, the growth rate was significantly decreased probably due to the competitive growth of 3D islands. For the

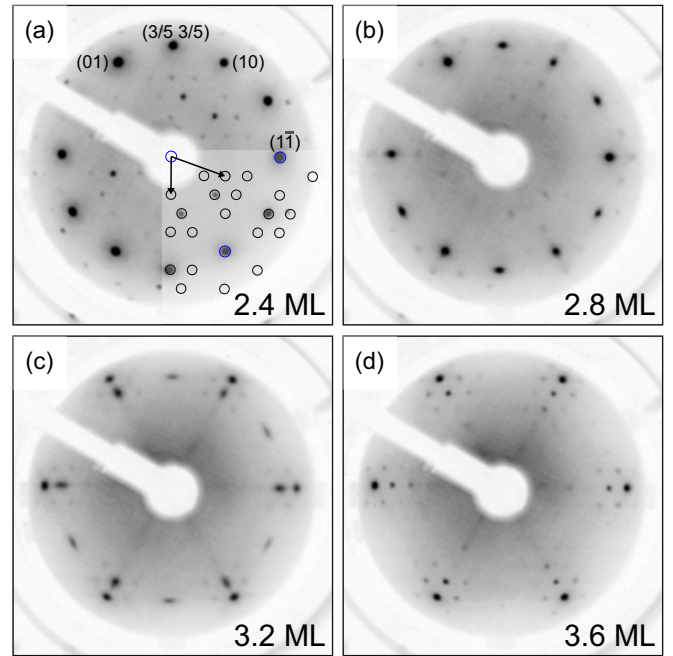


FIG. 1. LEED patterns from (a) a pristine In/Si(111)- $(\sqrt{7} \times \sqrt{3})$ surface (2.4 ML) and (b)–(d) after the additional deposition of In (0.4, 0.8, and 1.2 ML). These patterns were taken with 78-eV electrons at 88 K. The open circles in (a) present the simulated reciprocal lattice points of the triple-domain $\sqrt{7} \times \sqrt{3}$ structure.

In deposition in the STM chamber, we needed to take out the sample from a cold stage at 78 K. We adjusted to minimize the total time that a sample was on the manipulator, and carefully checked the consistency with the LEED experiments. For ARPES measurements, we grew the triple-layer structure at 80–100 K and applied moderate postannealing up to 140 K for a few minutes in order to improve the crystallinity as described later [Fig. 3(b)].

III. RESULT

Figures 1(a)–1(d) show LEED pattern change with increasing In coverage from the In/Si(111)-rect structure at 88 K. Most fractional spots of the triple-domain $(\sqrt{7} \times \sqrt{3})$ superlattice, described by a matrix notation $(1-1|23)$ with respect to the Si(111) (1×1) lattice, are clearly seen in Fig. 1(a), indicating a well-ordered double-layer structure. Among them, the $(\frac{2}{5} \frac{3}{5})$ and equivalent spots are particularly intense, and thus, are considered to be a good criterion for the completion of an upper layer. While additional deposition of In weakened the intensity of the $(\sqrt{7} \times \sqrt{3})$ spots, several new spots gradually became visible around the (1×1) spots. At the total coverage of 3.6 ML, the $(\sqrt{7} \times \sqrt{3})$ pattern completely disappeared except for the spots from Si(111)- (1×1) and the newly appeared sharp spots constitute a hexagonal pattern.

Among the newly appeared spots, six spots outside of the Si(111)- (1×1) spots are considerably intense. This LEED pattern was observed at different electron energies in 70–120 eV, indicating that these spots are not due to 3D islands of In. The in-plane scattering vector of the most intense spots ($k_{\parallel} = 2.2 \text{ \AA}^{-1}$) is $\sim \frac{7}{6}$ times as long as that of

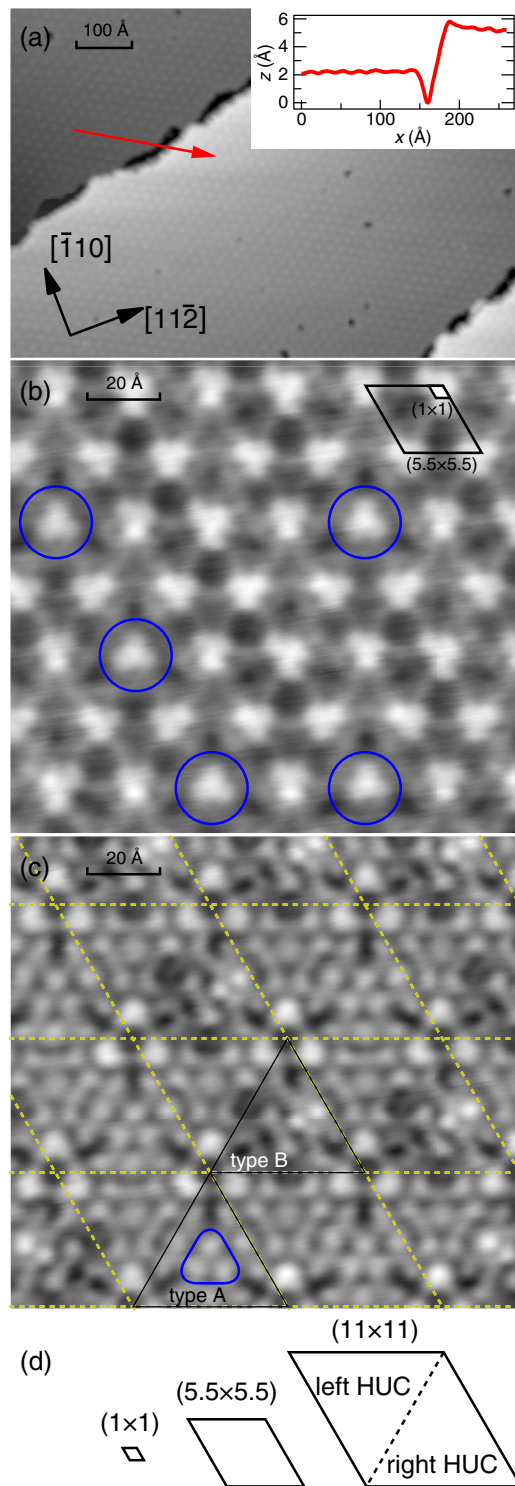


FIG. 2. (a) A wide-area STM image of the triple-layer structure taken at sample bias $V_s = -1.0$ V and tunnel current $I = 0.1$ nA. The inset shows the height profile along the arrow crossing the step edge. Closeup STM images of the same area taken at (b) $V_s = -1.0$ and $I = 0.5$ nA, and (c) $V_s = +0.5$ V and $I = 0.5$ nA. The grid pattern represents the (11×11) lattice. (d) The unit cells of (1×1) , (5.5×5.5) , and (11×11) depicted in the same scale as (b) and (c). The STM images were recorded at 78 K for (a) and 5 K for (b) and (c).

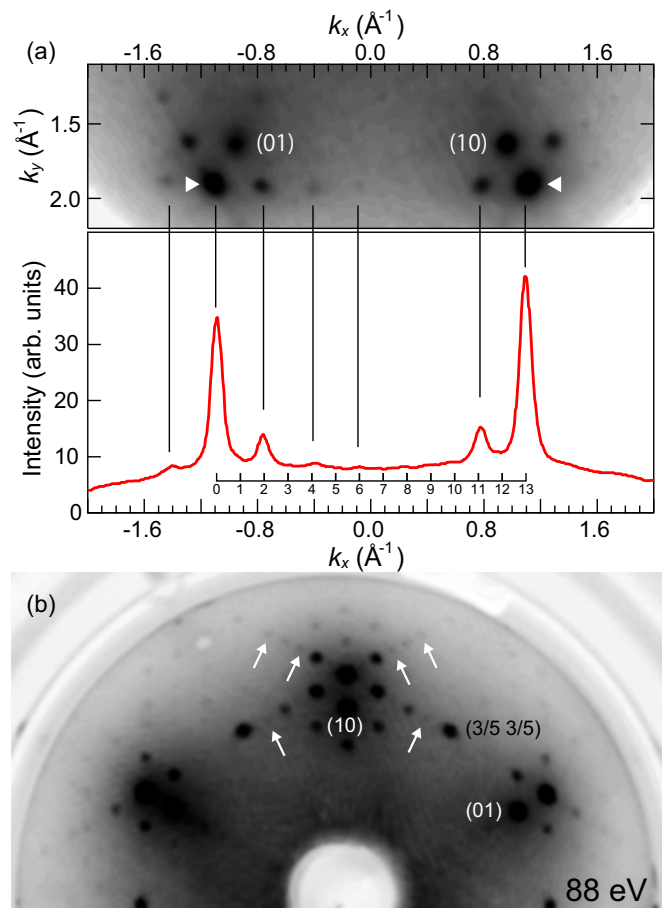


FIG. 3. (a) The upper panel presents the LEED pattern from the triple-layer structure taken with 90-eV electrons, and the lower panel the intensity profile on the line indicated by the triangles in the upper panel. (b) The LEED pattern from the triple-layer structure taken with 88-eV electrons.

Si(111) (1×1) (1.89 \AA^{-1}) , which indicates that this phase corresponds to the (6×6) structure reported by the previous low-energy electron microscopy (LEEM)/LEED and STM studies [20,21]. Assuming that each layer contains 1.2 ML as the $\sqrt{7} \times \sqrt{3}$ -rect structure, the total coverage amounts to 3.6 ML, which is reasonable for a triple-layer structure. The superstructure spots are seen only around the (1×1) spots, which is typical for incommensurate and high-order commensurate structures [25,26].

Figure 2(a) is a STM image of the surface covered with the triple-layer structure. A uniform hexagonal array of spots is seen over a whole 500-Å-wide terrace. Although there are a small amount of pointlike defects, domain boundary defects are not found on the wide terrace. The line profile crossing a step edge shows that the step height is same as that on Si(111) (3.1 \AA) . The apparent corrugation of the spots of the triple-layer structure is only $\sim 0.16 \text{ \AA}$, indicating that the surface is atomically flat. The spots are aligned along the $[1\bar{1}0]$ and $[10\bar{1}]$ directions, and their interval is $20.7 \pm 0.4 \text{ \AA}$. The period of the spots is consistent with $5.5a_{\text{Si}}$ rather than $6a_{\text{Si}}$. Figure 2(b) shows a closeup image of the triple-layer structure, where a (5.5×5.5) unit cell is also indicated. In

this image, each spot in the wide-area image turns out to be a triangle-shaped structure or a trimer of smaller spots. This shape is consistent with that observed in the previous STM study of the same surface, which was, however, referred to as the (6×6) structure [21]. We note a recent STM study showing the $(\sim 5.4 \times \sim 5.4)$ superstructure on In/Si(111). The lattice size is close to that we determined by our STM observation. However, the angle between the unit-cell vectors was reported to be smaller than 60° by 4° , indicating an oblique lattice. Our LEED observation of the triple-layer structure does not show such distortion from the hexagonal lattice.

A closer look at Fig. 2(b) revealed disorder in direction of the triangles; most of the triangles point downward, but some point upward. The latter are indicated by the open circles. The arrangement that the five upward triangles are lined up at a same interval ($\sim 41 \text{ \AA}$) implies a hidden lattice whose size is twice (5.5×5.5) , that is, (11×11) [Fig. 2(d)]. The (11×11) periodicity became evident when the bias voltage was changed from negative to positive, as shown in Fig. 2(c). The most characteristic feature observed at $V_s = +0.5 \text{ V}$ is dark spots, each of which is surrounded by three bright spots. The (11×11) grid pattern is drawn as each cross point is located at the dark spot. The (11×11) unit cells appear to contain about 20 spots. It is helpful to recognize the configurations of the spots separately for the left and right half-unit cells (HUCs) [Fig. 2(d)]. The spot configuration of the left HUCs is identical to each other. On the other hand, the right HUCs have two types of configurations; one has a threefold symmetry [type A in Fig. 2(c)], and the other has no rotational symmetry and fewer spots (type B). As to the type-A HUCs, central trimerlike features, one of which is indicated by a rounded triangle in Fig. 2(c), correspond to the upward triangles at $V_s = -1.0 \text{ V}$. Because the two types of the right HUCs were distributed randomly, the configurational entropy of mixing may contribute to the stability of the triple-layer structure. However, the coexistence of the different local structures does not disturb the periodicity of the (11×11) lattice. Therefore, the (11×11) LEED spots are expected to be sharp, which is consistent with our LEED observation.

Now we analyze the observed LEED pattern in detail. Figure 3(a) shows the LEED pattern of the triple-layer structure taken at 90 eV. The k_x and k_y axis were scaled by the Si (1×1) spots. An array of seven spots are seen on a horizontal line at $k_y = 1.9 \text{ \AA}^{-1}$. The intensity line profile on the line is shown in the lower panel. The average distance between spots in close proximity was measured to be $0.34 \pm 0.03 \text{ \AA}^{-1}$. A corresponding lattice constant of a hexagonal lattice is 21.7 \AA , whose ratio to 3.84 \AA of Si(111) (1×1) is 5.6 ± 0.2 . Assuming the (11×11) superlattice, the indices of the two intense spots in the line profile are $(13/11 \ 0)$ and $(0 \ 13/11)$. In Fig. 3(a), a ruler is drawn with 14 ticks placed with an equal spacing. All the observed spots are found to be located on the ticks. In further experiments, we found that moderate annealing at $\sim 140 \text{ K}$ improved the crystalline quality of the triple-layer structure. The LEED pattern [Fig. 3(b)] from the sample made in this way exhibits much more spots compared to Figs. 1(d) and 3(a). Some of the newly observed spots are indicated by the white arrows. They are all consistent with a (11×11) reciprocal lattice.

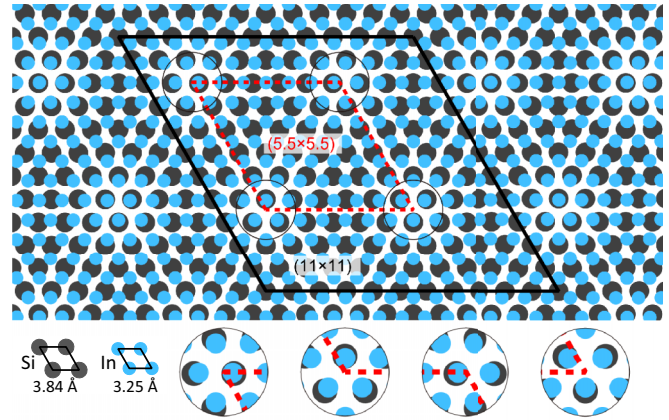


FIG. 4. A schematic model showing the topmost hexagonally packed In layer on Si(111). Black circles are Si atoms, and light-blue circles are In atoms. (11×11) and (5.5×5.5) unit cells are represented by the solid and dotted (red) rhombi, respectively. The closeup images near each corner of the (5.5×5.5) unit cell are shown at the bottom.

In Fig. 3(b), the $(\frac{3}{5} \ \frac{3}{5})$ and equivalent spots are also seen, showing that the $\sqrt{7} \times \sqrt{3}$ -rect structure was partially exposed by the moderate annealing. Thermally removed In atoms must be incorporated into 3D crystals of In as reported in the previous LEEM study [20]. This behavior was observed to proceed rapidly in a short period, typically several minutes, above 140 K. However, it was not detected below 100 K for hours. It should be noted that the $(\frac{3}{5} \ \frac{3}{5})$ spot is located in close proximity to the center between the intense $(13/11 \ 0)$ and $(0 \ 13/11)$ spots, which corresponds to the point scaled 6.5 on the ruler in Fig. 3(a). This shows the fact that the $(\sqrt{7} \times \sqrt{3})$ lattice and the (11×11) one do not have a commensurate relation.

Structure models of close-packed atomic layers as fcc or hcp were considered in the previous studies [20,21]. Now we examine a similar structure model (Fig. 4) taking into consideration the lattice matching between $11a_{\text{Si}}$ and $13a_{\text{In}}$, where a_{In} is assumed to be 3.25 \AA . In this figure, only the topmost In atoms and the Si(111) atoms are depicted with the orientation being identical to each other. The difference in periodicity between the Si and In layers yields a moiré pattern with the (5.5×5.5) pseudoperiodicity, which is easily recognized by focusing areas where the white color of the background is noticeable. This graphical feature reflects the difference in the registry of the In atoms with respect to the Si atoms. The atom configurations of both HUC in this model have threefold symmetry, which is consistent with the high-symmetry pair of HUCs observed in the STM image [Fig. 2(c)]. Note that the atomic arrangement at the lattice points of (5.5×5.5) is not exactly the same with each other (see the bottom images in Fig. 4), which is why the (5.5×5.5) is a pseudoperiodicity. Consequently, the (5.5×5.5) patterns observed by LEED and STM, respectively, are interpreted as reflecting the moiré modulation.

Figure 5(a) shows a FS map of the (11×11) structure measured by ARPES at 80 K. In order to make the pattern of the FS clear, the original ARPES data in a 60° range from

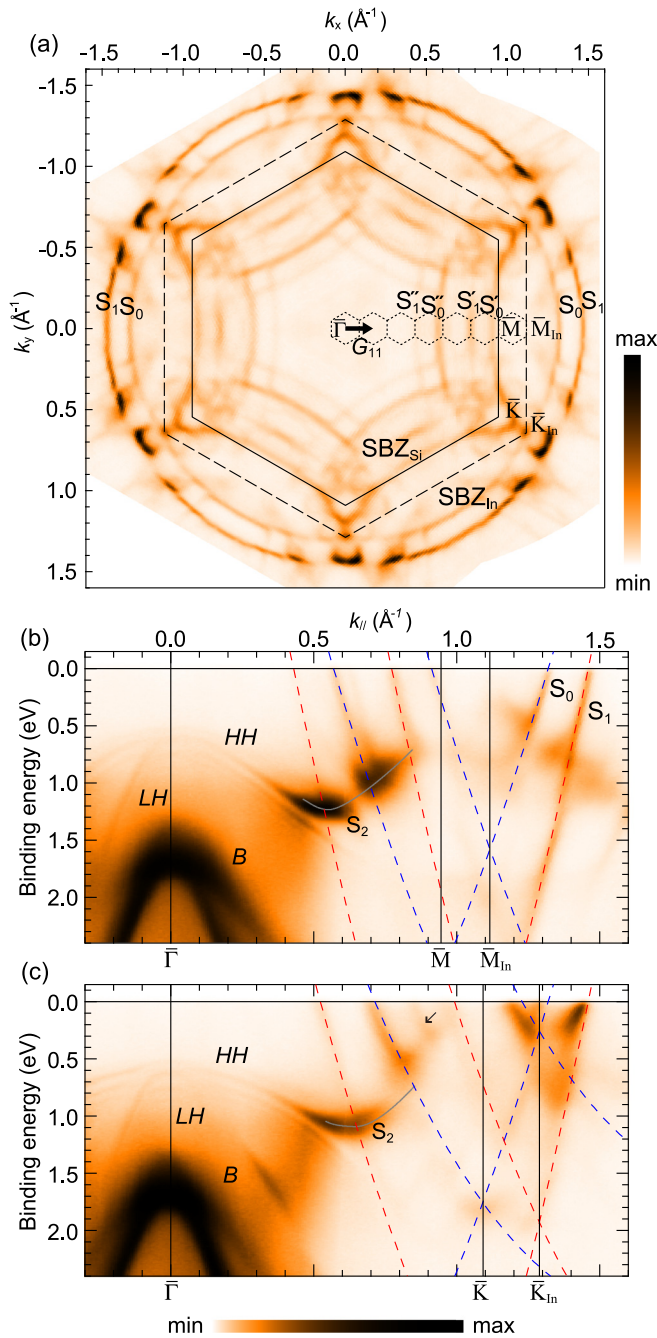


FIG. 5. (a) A Fermi-surface map of the triple-layer structure on In/Si(111) where ARPES intensity was averaged within an energy window of 40 meV centered at E_F . The solid, dotted, and dashed hexagons represent the SBZs of Si(111) (1×1), (11×11) and the close-packed layer with an atomic distance of 3.25 \AA , respectively. The bold arrow is a primitive (11×11) reciprocal lattice vector \mathbf{G}_{11} . ARPES band dispersion maps along (b) $\bar{\Gamma}$ - \bar{M} and (c) $\bar{\Gamma}$ - \bar{K} of the Si(111) (1×1) SBZ. The dashed curves are fitted free-electron dispersion relations with the offset by reciprocal lattice vectors. The solid curves indicate the experimental dispersions of S_2 and S'_2 .

$\bar{\Gamma}$ - \bar{M} to $\bar{\Gamma}$ - \bar{K} is symmetrized by reflection and rotation of 120° . Note that the Si(111) mirror plane is on $\bar{\Gamma}$ - \bar{M} , not on $\bar{\Gamma}$ - \bar{K} . The two large hexagons represent the first surface Brillouin zones (SBZs) of Si(111) (1×1) and the hexagonal layer

with an atomic distance of 3.25 \AA . In-derived FSs are seen as multiple circles and warped hexagons. The most striking feature is large two circular FSs (S_0 and S_1) located outside of the first In-layer SBZ (SBZ_{In}). These states are attributed to 2D free-electron-like states. The Fermi wave vectors of the inner and outer FSs are 1.32 and 1.46 \AA^{-1} , respectively, in the extended zone scheme.

Other remarkable FS features are FS arcs, labeled S'_0 , S'_1 , S''_0 , and S''_1 , inside the first SBZ_{In} , which appears to form warped hexagons. Each FS arc has the same curvature of S_0 or S_1 . For example, S'_0 and S'_1 near $(0.8 \text{\AA}^{-1}, 0)$ coincide perfectly with S_0 and S_1 near $(-1.4 \text{\AA}^{-1}, 0)$, respectively, by the translation of a reciprocal lattice vector $13|\mathbf{G}_{11}| = |\mathbf{G}_{In}|$, where $|\mathbf{G}_{11}| = 0.17 \text{\AA}^{-1}$ and $|\mathbf{G}_{In}| = 2.23 \text{\AA}^{-1}$. The same holds for S''_0 and S''_1 near $(0.5 \text{\AA}^{-1}, 0)$ by translation of $11|\mathbf{G}_{11}| = |\mathbf{G}_{Si}|$, where $|\mathbf{G}_{Si}| = 1.89 \text{\AA}^{-1}$. These relations are more easily recognized by reflecting S_0 or S_1 with respect to the SBZ_{In} and the Si(111) (1×1) SBZ (SBZ_{Si}) boundaries. Observation of replica bands by ARPES is often related to surface umklapp scattering of photoemission final states [27,28]. This interpretation is reasonable because anticrossing behavior is not found in the FS map. However, if hybridization gaps of the metallic bands were small (\lesssim a few tens meV), it is difficult to distinguish whether each FS arc is attributed to umklapp scattering or to an initial state.

Figures 5(b) and 5(c) show ARPES band maps of the (11×11) structure along $\bar{\Gamma}$ - \bar{M} and $\bar{\Gamma}$ - \bar{K} , respectively. We fit the S_0 and S_1 band dispersions along $\bar{\Gamma}$ - \bar{M} with free-electron dispersion relation, that is, $E = \hbar^2 k^2 / 2m^* + E_0$, where m^* is an effective mass and E_0 an energy offset. Fitting parameters are only m_i^* because E_0 was determined by the measured Fermi wave vectors $k_{F,i}$ ($i = 0, 1$) (1.32 \AA^{-1} for S_0 and 1.46 \AA^{-1} for S_1). As a result of the fittings, we obtained $m^* = 0.93m_e$ for S_0 and $1.2m_e$ for S_1 , where m_e is the free-electron mass. The fitting curves and their replica bands derived in the empty lattice approximation with \mathbf{G}_{Si} and \mathbf{G}_{In} are drawn as dashed curves in Figs. 5(b) and 5(c). This simple model shows a good agreement for most of the observed metallic band dispersions. For the $\bar{\Gamma}$ - \bar{K} direction, the fitting curve is slightly deviated from the experimental dispersions, showing weak anisotropy of the metallic states of the (11×11) structure. In Fig. 5(c), no corresponding free-electron band was found for a weak feature indicated by the arrow at 0.9\AA^{-1} . This band is probably attributed to minor $\sqrt{7} \times \sqrt{3}$ -rect domains unintentionally recovered by postannealing as observed by LEED [Fig. 3(b)].

In Figs. 5(b) and 5(c), the Si bulk band (labeled B) and the hole subbands (HH and LH) are observed to disperse downward away from $\bar{\Gamma}$. The subbands are attributed to quantum states confined by upward band bending in the near-interface region of n -type Si [29]. The valence band maximum of the Si substrate was estimated to be at 0.5 eV from the leading edge of the subband feature. When one follows the topmost HH subband away from $\bar{\Gamma}$, the subband feature is transferred to another band, labeled S_2 at ~ 1 eV and 0.5\AA^{-1} in both directions. This would be attributed to the change of the orbital character from $p_x + p_y$ to p_z [30,31]. The p_z -like state on Si(111) is typically related to the dangling bond state.

The replica pattern of the 2D free-electron-like FS was discussed in the ARPES study of the double-layer $\sqrt{7} \times \sqrt{3}$ -rect

structure [4]. The $\sqrt{7} \times \sqrt{3}$ -rect structure has a single circular FS with $k_F = 1.4 \text{ \AA}^{-1}$. The replica FSs are characterized by reciprocal lattice vectors associated with the pseudo-fourfold geometry of the In atoms. This is due to that the photoemission matrix elements are sensitive to electron distribution in the vicinity of the emitting atoms. As for the (11×11) structure, the pattern of the observed FSs (S'_0 and S'_1) was related to the hexagonal lattice whose lattice constant is 3.25 \AA . We believe that this result provides support for our hexagonal-layer model (Fig. 4).

Recently, similar double-circular FSs have been reported for the (In, Mg)/Si(111)-($\sqrt{3} \times \sqrt{3}$) structure [31]. The measured values of k_F are 1.29 and 1.46 \AA^{-1} , which are very close to those on the (11×11) structure (1.32 and 1.46 \AA^{-1}). This (In, Mg)/Si(111) structure was fabricated by Mg deposition on the $\sqrt{7} \times \sqrt{3}$ -rect structure at $\sim 200 \text{ K}$. First-principles total-energy calculations revealed that the structure consists of three hexagonally packed atomic layers, each of which contains $\frac{4}{3}$ ML atoms, in ABC stacking order. Most of Mg atoms are incorporated to the bottom layer to terminate the dangling bonds on Si(111) and ionized, and therefore, the free-electron-like 2D states are mainly derived from In valence orbitals. In general, confinement of electrons in an ultrathin film leads to quantum well states when film thickness is several times thicker than the Fermi wavelength. However, because the (In, Mg) triple-layer structure is too thin, the metallic states are rather described in terms of local bonding; metallic states are split into a bonding-antibonding pair according to the presence or absence of nodes. This is the origin of the double circular FSs.

Finally, we discuss about the atomic structure of the triple-layer structure of In/Si(111). A straightforward model is that the third hexagonal In layer is on the double-layer $\sqrt{7} \times \sqrt{3}$ -rect structure. Assumed that the coverage of $(13/11)^2 \sim 1.40$ ML for the third layer (Fig. 4), the total coverage of this model is $2.4 + 1.4 = 3.8$ ML, which roughly agrees with the experimental coverage of 3.6 ML. Although the (11×11) lattice is not commensurate with the $(\sqrt{7} \times \sqrt{3})$ one, such structure seems likely, given the incommensurate structure of the single-layer hex structure on Si(111) [11]. Nevertheless, our LEED and ARPES results raise questions. The 12 intense spots in the $\sqrt{7} \times \sqrt{3}$ -rect LEED pattern [Fig. 1(a)] are considered as a combination of three 120° -rotated virtual square reciprocal lattices, for example, one of which is formed by the pair of the orthogonal $(00) - (\frac{3}{5}, \frac{3}{5})$ and $(00) - (1\bar{1})$ vectors. This feature reflects the nearly square atom arrangement of the double-layer structure with the lateral atomic distances of $\sim 3.3 \text{ \AA}$. If the quasisquare arrangement was preserved under the third hexagonal layer, it is expected that the relatively intense LEED spots with hexagonal symmetry appear around the $(\frac{3}{5}, \frac{3}{5})$ and equivalent reciprocal lattice points by double scattering. Actually, the (11×11) spots were observed only around the Si(111) (1×1) spots [Fig. 1(d)]. Besides, the replica pattern of the FSs observed by ARPES also showed

no square-lattice features. These results indicate that the formation of the triple-layer structure is accompanied by the reconstruction of the underlying In layers. In the previous study of slightly thicker In films (6–8 layers) on Si(111), the structural change from fcc (hexagonal) to bct (tetragonal) was found during the growth at $< 100 \text{ K}$ [24]. Therefore, it is expected that there is no significant difference in stability between the square and hexagonal structures for ultrathin In films, and the barrier is so small that the transition occurs in as-deposited films at $\sim 100 \text{ K}$.

Here we propose a model in which two hexagonal close-packed layers are present as the upper two layers. This model is based on the close similarity of the Fermi surfaces between the In and the (In, Mg) triple-layer structures [31]. The packing density (1.40 ML) in a hexagonal layer of our (11×11) model (Fig. 4) is slightly higher than $\frac{4}{3}$ ML of the (In, Mg)/Si(111) structure. Although the difference yields a smaller atomic distance by 0.07 \AA in the (11×11) structure, it is possibly compensated by vertical corrugation of atomic positions. As to the bottom layer, the packing density is calculated to be 0.8 ML from the total coverage of 3.6 ML. However, underestimation of the coverage is possible because the LEED experiments to determine a deposition rate were done for Si(111) at room temperature where the sticking probability of In atoms is expected to be lower than the temperature ($\sim 100 \text{ K}$) during the growth of the (11×11) structure. Thus, the total coverage of the triple-layer structure may be closer to 4 ML than 3.6 ML. Considering the termination of the Si(111) substrate in the $\sqrt{7} \times \sqrt{3}$ -rect structure, a packing density of 1.2 ML is sufficient. Electron-density profile analysis by surface x-ray diffraction is suitable for examining our model [32].

IV. SUMMARY

We performed the experimental study of the triple-layer structure by LEED, STM, and ARPES. Although the structure was referred to as (6×6) in the previous studies, the superlattice was determined to be (11×11) . The half-period moiré pattern emphasized in LEED and STM observations is explained by the overlap of the Si(111) lattice and the overlayer lattice of hexagonally packed In atoms. The electronic structure of the (11×11) structure is characterized by two 2D free-electron-like states. Compared to the $\sqrt{7} \times \sqrt{3}$ -rect structure, these states are expected to have less contribution of dangling bond states on Si(111), thus, the triple-layer structure can provide more insight into electronic properties of free-standing 2D metals and probably of 2D superconductivity.

ACKNOWLEDGMENTS

This work was financially supported by JSPS KAKENHI (Grants No. 21K03432, No. 21H01886, No. 21K18202, and No. 22K05036) and JST CREST (Grant No. JPMJCR20R4).

[1] S. Qin, J. Kim, Q. Niu, and C.-K. Shih, *Science* **324**, 1314 (2009).

[2] L. Aballe, A. Barinov, A. Locatelli, S. Heun, and M. Kiskinova, *Phys. Rev. Lett.* **93**, 196103 (2004).

- [3] A. Politano and G. Chiarello, *Prog. Surf. Sci.* **90**, 144 (2015).
- [4] E. Rotenberg, H. Koh, K. Rossnagel, H. W. Yeom, J. Schäfer, B. Krenzer, M. P. Rocha, and S. D. Kevan, *Phys. Rev. Lett.* **91**, 246404 (2003).
- [5] S. Yamazaki, Y. Hosomura, I. Matsuda, R. Hobarra, T. Eguchi, Y. Hasegawa, and S. Hasegawa, *Phys. Rev. Lett.* **106**, 116802 (2011).
- [6] T. Zhang, P. Cheng, W.-J. Li, Y.-J. Sun, G. Wang, X.-G. Zhu, K. He, L. Wang, X. Ma, X. Chen, Y. Wang, Y. Liu, H.-Q. Lin, J.-F. Jia, and Q.-K. Xue, *Nat. Phys.* **6**, 104 (2010).
- [7] T. Uchihashi, P. Mishra, M. Aono, and T. Nakayama, *Phys. Rev. Lett.* **107**, 207001 (2011).
- [8] J. W. Park and M. H. Kang, *Phys. Rev. Lett.* **109**, 166102 (2012).
- [9] J. W. Park and M. H. Kang, *Phys. Rev. Lett.* **117**, 116102 (2016).
- [10] T. Shirasawa, S. Yoshizawa, T. Takahashi, and T. Uchihashi, *Phys. Rev. B* **99**, 100502(R) (2019).
- [11] S. Terakawa, S. Hatta, H. Okuyama, and T. Aruga, *Phys. Rev. B* **100**, 115428 (2019).
- [12] S. Yoshizawa, T. Kobayashi, Y. Nakata, K. Yaji, K. Yokota, F. Komori, S. Shin, K. Sakamoto, and T. Uchihashi, *Nat. Commun.* **12**, 1462 (2021).
- [13] M. S. Finney, C. Norris, P. B. Howes, R. G. van Silfhout, G. F. Clark, and J. M. C. Thornton, *Surf. Sci.* **291**, 99 (1993).
- [14] O. Bunk, G. Falkenberg, J. H. Zeysing, L. Lottermoser, R. L. Johnson, M. Nielsen, F. Berg-Rasmussen, J. Baker, and R. Feidenhans'l, *Phys. Rev. B* **59**, 12228 (1999).
- [15] S. Terakawa, S. Hatta, H. Okuyama, and T. Aruga, *J. Phys.: Condens. Matter* **30**, 365002 (2018).
- [16] K. Uchida and A. Oshiyama, *Phys. Rev. B* **87**, 165433 (2013).
- [17] S. Yoshizawa, H. Kim, T. Kawakami, Y. Nagai, T. Nakayama, X. Hu, Y. Hasegawa, and T. Uchihashi, *Phys. Rev. Lett.* **113**, 247004 (2014).
- [18] S. L. Surnev, J. Kraft, and F. P. Netzer, *J. Vac. Sci. Technol. A* **13**, 1389 (1995).
- [19] J. Kraft, M. G. Ramsey, and F. P. Netzer, *Phys. Rev. B* **55**, 5384 (1997).
- [20] A. Pavlovskaya, E. Bauer, and M. Giessen, *J. Vac. Sci. Technol. B* **20**, 2478 (2002).
- [21] M. Xu, X.-M. Dou, J.-F. Jia, Q.-K. Xue, Y. Zhang, A. Okada, S. Yoshida, and H. Shigekawa, *Thin Solid Films* **520**, 328 (2011).
- [22] T. Suzuki and K. Yagyu, *Surf. Sci.* **726**, 122174 (2022).
- [23] J. Chen, M. Hupalo, M. Ji, C. Z. Wang, K. M. Ho, and M. C. Tringides, *Phys. Rev. B* **77**, 233302 (2008).
- [24] J. H. Dil, B. Hülsen, T. U. Kampen, P. Kratzer, and K. Horn, *J. Phys.: Condens. Matter* **22**, 135008 (2010).
- [25] A. T. N'Diaye, J. Coraux, T. N. Plasa, C. Busse, and T. Michely, *New J. Phys.* **10**, 043033 (2008).
- [26] D. Martocchia, P. R. Willmott, T. Brugger, M. Björck, S. Günther, C. M. Schlepütz, A. Cervellino, S. A. Pauli, B. D. Patterson, S. Marchini, J. Wintterlin, W. Moritz, and T. Greber, *Phys. Rev. Lett.* **101**, 126102 (2008).
- [27] H.-J. Neff, I. Matsuda, M. Hengsberger, F. Baumberger, T. Greber, and J. Osterwalder, *Phys. Rev. B* **64**, 235415 (2001).
- [28] J. N. Crain, K. N. Altmann, C. Bromberger, and F. J. Himpsel, *Phys. Rev. B* **66**, 205302 (2002).
- [29] S. N. Takeda, N. Higashi, and H. Daimon, *Phys. Rev. Lett.* **94**, 037401 (2005).
- [30] S. D. Stolwijk, A. B. Schmidt, M. Donath, K. Sakamoto, and P. Krüger, *Phys. Rev. Lett.* **111**, 176402 (2013).
- [31] S. Terakawa, S. Hatta, H. Okuyama, and T. Aruga, *Phys. Rev. B* **105**, 125402 (2022).
- [32] T. Shirasawa, M. Ohyama, W. Voegeli, and T. Takahashi, *Phys. Rev. B* **84**, 075411 (2011).